LETTERS
PUBLISHED ONLINE: 2 JUNE 2013 | DOI: 10.1038/NPHYS2631
nature physics

Deterministic quantum teleportation between distant atomic objects

H. Krauter[1], D. Salart[1], C. A. Muschik[2], J. M. Petersen[1], Heng Shen[1], T. Fernholz[3] and E. S. Polzik[1]*

Quantum teleportation is a key ingredient in quantum networks[1,2] and one of the building blocks for quantum computation[3,4]. Teleportation between distant material objects using light as the quantum-information carrier has been a particularly exciting goal. Here we propose and demonstrate the deterministic continuous-variable teleportation between distant material objects. The objects are macroscopic atomic ensembles at room temperature. Entanglement required for teleportation is distributed by light propagating from one ensemble to the other. We demonstrate that the experimental fidelity of the quantum teleportation is higher than that achievable by any classical process. Furthermore, we demonstrate the benefits of deterministic teleportation by teleporting a sequence of spin states evolving in time from one distant object onto another. The teleportation protocol is applicable to other important systems, such as mechanical oscillators coupled to light or cold spin ensembles coupled to microwaves.

Quantum teleportation of discrete[5] and continuous[6] variables is the transfer of a quantum-mechanical state without the transmission of a physical system carrying this state. The first experimental teleportation protocols employed light as the carrier of quantum states[7,8]. Teleportation of atomic states over micrometre distances has been realized in two experiments using short-range interactions between trapped ions[9,10]. Interspecies teleportation from light onto atoms has been achieved both deterministically for continuous variables[11] and probabilistically for discrete variables[12]. Recently, probabilistic teleportation between two ions[13], atoms[14] and atomic ensembles[15] over a macroscopic distance has been demonstrated. Whereas probabilistic teleportation, in which entanglement is distributed by photon counting[7,16], is capable of reaching distances of many kilometres (refs 2,17), the power of continuous-variable teleportation is that it succeeds deterministically in every attempt[8,11], that it is capable of teleporting complex quantum states[18] and that it can be used in universal quantum computation[4]. Here, we propose and experimentally demonstrate the deterministic continuous-variable teleportation between two distant material objects, thus extending the powerful continuous-variable teleportation[8,11,18] onto atomic memory states. The protocol that succeeds in every attempt allows us to teleport dynamically changing quantum states of collective atomic spins with the bandwidth of tens of hertz.

A quantum teleportation process begins with the creation of a pair of entangled objects. In our experiment these two objects are an atomic ensemble at site B and a photonic wave packet generated by interaction of this ensemble with a driving light pulse (Fig. 1a). The wave packet travels to site A, the location of the atomic ensemble whose state is to be teleported. This step establishes a quantum link between the two locations. Following the interaction of ensemble A and the wave packet, a measurement is performed on the transmitted light. The results of this measurement are communicated through a classical channel to site B, where they are fed back through local operations on the second entangled object, that is, ensemble B, thus completing the process of teleportation.

Continuous-variable teleportation is described in the language of canonical operators x, p for atoms and y, q for light that obey the usual commutation relations $[x, p] = [y, q] = i$. A generic condition for a continuous-variable entangled state for Gaussian states[19] is $\mathrm{Var}(x - y) + \mathrm{Var}(p + q) < 2$. For atomic ensembles, fully spin polarized along the x axis, canonical operators are scaled dimensionless Cartesian components of the collective spin: $x = J_y/\sqrt{|\langle J_x\rangle|}$ and $p = J_z/\sqrt{|\langle J_x\rangle|}$ (ref. 19), where $J_{x,y,z} = \sum_i j^i_{x,y,z}$ (summed over all atoms i) is the collective angular momentum of the ensemble. Here, we employ ^{133}Cs atoms initiated in a fully polarized $|F = 4, m_F = 4\rangle$ ground state. The usual link between the ladder operator b for collective atomic excitations[19] of the state $m_F = 3$ (Fig. 1b) and canonical variables is $b^\dagger = (x - ip)/\sqrt{2}$. Atoms are placed in a bias magnetic field along the x axis, so that in the laboratory frame the observables $x \propto J_y$ and $p \propto J_z$ rotate at the Larmor frequency Ω (Fig. 1a) according to the atomic Hamiltonian $H_{\mathrm{Atomic}} = -\Omega(x^2 + p^2)/2$. Note that here we use the parallel orientation of the macroscopic spins of the two ensembles (Fig. 1a), which is optimal for the teleportation protocol. It corresponds to the same sign of the Larmor frequency Ω in H_{Atomic} for the two ensembles. This is to be compared to[19,20] where the antiparallel spin orientation, optimal for creating entanglement between two atomic spin ensembles, was used.

The atom–light interaction is shown in Fig. 1b and involves two scattering processes $H_{\mathrm{int}} \propto \nu a^\dagger_{\mathrm{us}} b^\dagger - \mu a^\dagger_{\mathrm{ls}} b + \mathrm{h.c.}$, where $a^\dagger_{\mathrm{us/ls}}$ generate photons in the upper/lower $(\omega_0 \pm \Omega)$ sideband modes of the driving field ω_0. The interaction H_{int} contains both essential ingredients of the teleportation protocol, the creation of entanglement (the first term) and a beam-splitter-type operation between atoms and photons (the second term)[19,20]. For our setting, the ratio of the two terms is $\mu/\nu = 1.38$. The entanglement used in this protocol is between atomic ensemble B and the light field sent to ensemble A. The photons scattered forward into Larmor-frequency sidebands populate the modes relevant for teleportation whose canonical variables $y_{c,s}$ and $q_{c,s}$ are $y_c \cos(\Omega t) + y_s \sin(\Omega t) \propto a_{\mathrm{us}} e^{-i\Omega t} + a_{\mathrm{ls}} e^{i\Omega t} + \mathrm{h.c.}$ and similarly for q. The detailed theory of the protocol is presented in the Supplementary Information, where exact definitions and properties

[1]Niels Bohr Institute, Copenhagen University, Blegdamsvej 17, 2100 Copenhagen, Denmark, [2]ICFO-Institut de Ciències Fotòniques, Mediterranean Technology Park, 08860 Castelldefels (Barcelona), Spain, [3]School of Physics & Astronomy, The University of Nottingham, Nottingham NG7 2RD, UK.
*e-mail: polzik@nbi.dk

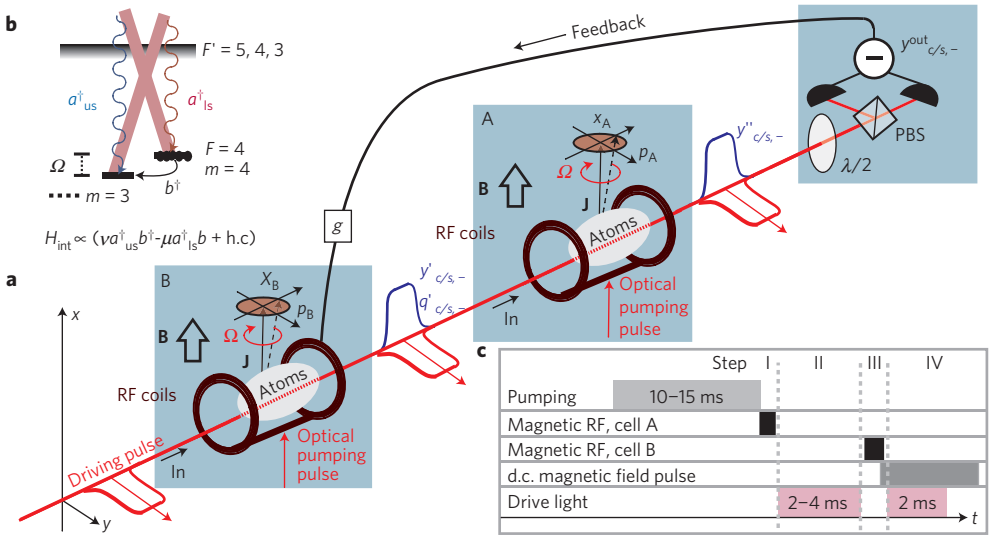

Figure 1 | Teleportation experiment. a, The experimental layout. A strong driving pulse propagates first through ensemble B creating the modes y', q' entangled with B and then through ensemble A whose state is to be teleported. Joint measurements on the modes y'' are performed using polarization homodyning. Teleportation is completed by classical communication of these results to B. See the text for further details. RF, radiofrequency. **b**, The level scheme and relevant transitions. Classical drive field (thick lines) and quantum fields forming the modes y, q (wavy lines) are shown. **c**, The time line of the experiment. I, preparation of the input state; II, entanglement and joint measurement; III, feedback; IV, read-out of the teleported state.

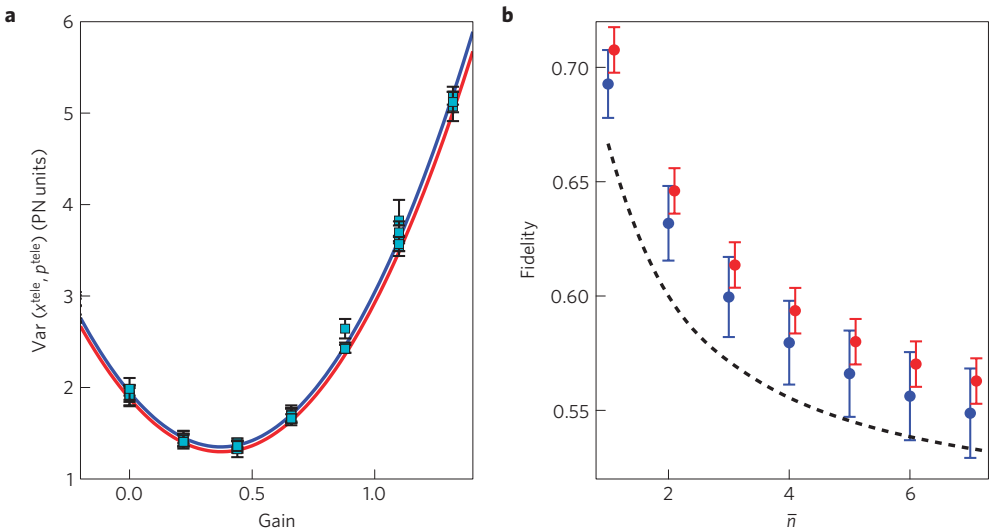

Figure 2 | Teleportation fidelity. a, The variances of the teleported state Var(x^{tele}, p^{tele}) in projection (vacuum) noise (PN) units as a function of gain. Several data points for each gain correspond to various input states (the vacuum, the CSS with displacements of 5 in vacuum units and phases 0, π/4, π/2 and CSS with displacement 25 and phase 0). The error bars represent one standard deviation of the atomic variance for 5–10 subsets of 2,000 points. **b**, Teleportation fidelity as a function of the mean photon number of the Gaussian distribution of the input set of states. Blue curves/points, feedback by radiofrequency pulses applied to ensemble B; red curves/points, feedback applied numerically to the read-out results of B (see comments in the text). Black dashed line represents the classical benchmark. For the error bars, the uncertainty of kappa, shot noise, detection efficiency and the quadratic fit of the atomic variance versus gain were taken into account.

of these modes are given in Supplementary Eqs S3 and S4). The generic form for them is $y_{c/s,f} \propto \int_0^T \cos/\sin(\Omega t) f(t) y(t) \mathrm{d}t$, where $f(t)$ is a function that varies slowly on the timescale of the Larmor period.

The experiment (Fig. 1a) uses two room-temperature gas ensembles of caesium atoms in glass cells with a spin-protecting coating as in ref. 19,21,22 placed at a distance of 0.5 m. Optical pumping initializes both ensembles into the $|F = 4, m_F = 4\rangle$ coherent spin state (CSS) with $\mathrm{Var}(J_y) \cdot \mathrm{Var}(J_z) = J_x^2/4$ with $J_x \approx 4N_A$ and $\langle J_y \rangle = 0$ and $\langle J_z \rangle = 0$, corresponding to a vacuum state with variances $\mathrm{Var}(x) = \mathrm{Var}(p) = 1/2$. The spin of ensemble A to be teleported is then displaced with mean values $\langle x_A \rangle$ and $\langle p_A \rangle$ by a weak radiofrequency magnetic field pulse of frequency Ω corresponding to the creation of a coherent superposition of electronic ground states $m_F = 3, m_F = 4$ (Fig. 1b).

The layout and the time sequence for teleportation and verification are shown in Fig. 1a,c. A y-polarized, 3-ms-long 5.6 mW light pulse, blue detuned from the D_2 line $F = 4 \rightarrow 5$ transition by $\Delta = 850$ MHz drives the interaction. The forward-scattered mode, x-polarized and described by y', q' is entangled with the collective spin B and co-propagates with the drive light towards site A. The interaction with ensemble A leads to partial mapping of its state onto light and is followed by the Bell measurements on the light modes of the upper and lower sidebands

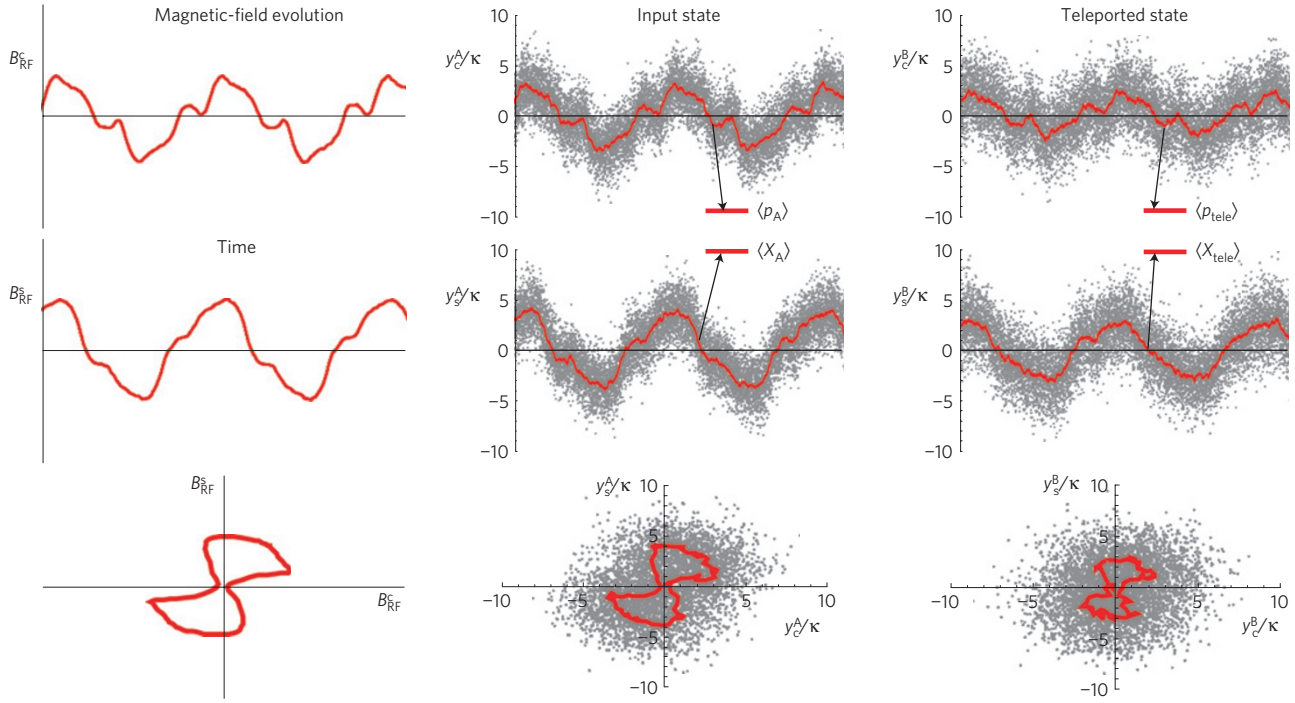

Figure 3 | Teleportation of a sequence of spin states. Left column, radiofrequency (RF) magnetic field applied to spin A with components $x_A \propto J_y \propto B^s_{RF}, p_A \propto J_z \propto B^c_{RF}$ with the amplitude of $B_{RF} \approx 1$ pT. Centre/right columns, the read-out of the input/teleported spin states A/B in vacuum units. Every point is one teleportation run with the points taken at the rate of ≈ 50 Hz with the whole shown sequence taking ≈ 200 s. The lines present the running average of the points. The first/second row in the read-out of the $p_{A,B}/x_{A,B}$ variable and the third row is a two-dimensional plot $x_{A,B}, p_{A,B}$. The optimal teleportation gain for this evolution is 0.8, which is seen as a smaller mean amplitude of the teleported evolution compared with the original.

performed using polarization homodyning with the driving light acting as the local oscillator yielding $y''_c = (y''_{us} + y''_{ls})/\sqrt{2}$ and $y''_s = (q''_{ls} - q''_{us})/\sqrt{2}$. The measurements of y''_c and y''_s serve as the joint measurement of ensemble A and the light coming from site B as can be seen directly from Supplementary Eq. S1. Near-unity teleportation fidelity can be achieved (see Supplementary Information), if the driving fields for the A and B ensembles are made time-dependent. However, even with top-hat driving pulses a sufficiently high fidelity can be achieved, if an optimal temporal mode for the detected homodyne signal is chosen. The optimal read-out mode is $y_{c/s,-} \propto \int_0^T \cos/\sin(\Omega t)\mathrm{e}^{-\gamma t} y(t)\mathrm{d}t$, where T is the pulse duration and γ is the decay rate of the atomic state. Measurements of $y_{c/s,-}$ are conducted by electronic processing of the photocurrent. The teleportation protocol is completed by sending the measurement results $y^{out}_{c/s,-}$ through a classical link to the site B where spin rotations in the y,z plane conditioned on these results are performed using phase- and amplitude-controlled radiofrequency magnetic field pulses at frequency Ω. The deterministic character of the homodyne process ensures success of the teleportation in every attempt.

The quantum character of the teleportation is verified by comparing the fidelity of state transfer to the classical benchmark fidelity. More specifically, we perform the teleportation using various sets of CSSs of ensemble A with varying $\langle J_{y,z} \rangle$, corresponding to displaced vacuum (coherent states) in quantum optical terms, as input states. For such states the individual state transfer fidelity is calculated from the first two moments (see Supplementary Information), that is, the mean values and the variances $\sigma_x^2 = \mathrm{Var}(x^{tele}_B)$, $\sigma_p^2 = \mathrm{Var}(p^{tele}_B)$. We then evaluate the average transfer fidelity for sets of coherent input states with a Gaussian distribution of displacements with a mean number of spin excitations[23] $\bar{n} = \langle b^\dagger b \rangle$ (see Supplementary Information). A rigorous classical benchmark fidelity $(1+\bar{n})/(1+2\bar{n})$ for transmission of such classes of states has been derived in ref. 23. Demonstration of a fidelity above the classical benchmark signifies the success of quantum teleportation and is equivalent to the ability of the teleportation channel to transfer entangled states. For every input state, 10,000–20,000 teleportations have been performed with one full cycle of the protocol lasting 20 ms. Figure 2a shows the variance of the teleported states as a function of gain g. The quadratic dependence of the variances on g predicted by the model (see Supplementary Information) fits the experimental data very well. For a certain range of g the atomic variances are reduced owing to the entanglement of the transmitted light with ensemble B (see Supplementary Information). Figure 2b presents the experimental fidelity (blue dots), which is above the classical benchmark for $\bar{n} \leq 7$. The classical feedback conditioned on the Bell measurement result can be applied in two ways. It can be done by performing a displacement operation with a radiofrequency pulse applied to ensemble B, followed by a subsequent verification by the read-out of the atomic state. Alternatively, the verification read-out can be performed first, followed by the displacement operation applied to the result of the measurement numerically (see Supplementary Information). In theory, those two procedures are equivalent, but in the experiment the resulting fidelity for the latter one is slightly higher (red dots in Fig. 2b) because the application of radiofrequency fields required in the former procedure introduces additional technical errors.

The deterministic teleportation can be used for stroboscopic teleportation of a sequence of spin states changing at a rate of ≈ 50 Hz from A to B. To illustrate this attractive feature, we have performed repeated teleportation cycles while varying the amplitude and phase of the input state. The results are presented in Fig. 3. The left column shows the time-varying radiofrequency field in the picoTesla range that is applied to prepare a new spin state A in each individual teleportation run, after initializing both ensembles to vacuum between the runs. The central column shows the read-out of the input-state evolution

of ensemble A and the right column shows the read-out of the teleported-state evolution. The points represent results for individual teleportation runs.

The fidelity of the teleportation can be further improved by using time-varying drive pulses (see Supplementary Information) and increasing the optical depth of the atomic ensembles. Continuous-variable teleportation is capable of teleporting highly non-classical states as shown for teleportation of light modes[18], so it can be expected that deterministic teleportation of an atomic qubit[16] can be performed by developing the present approach. The stroboscopic teleportation of spin dynamics can also be extended towards a true continuous in time teleportation paving the way to teleportation of quantum dynamics and simulations of the interaction between two distant objects that have never interacted directly (Muschik *et al.*, in preparation). Continuous-variable atomic teleportation allows for performing quantum sensing at a remote location, spatially separated from the location of the object. This teleportation protocol is, in principle, applicable to other systems described by strongly coupled harmonic oscillators, for example, to mechanical oscillators in a quantum regime coupled to light or cold spin ensembles coupled to microwaves.

Methods

The Larmor precession of the atomic spin oscillators in the bias magnetic field allows us to perform quantum teleportation with a very large atomic object consisting of $N_A \approx 10^{11}$–10^{12} atoms and to use a strong drive with the number of photons of $N_{ph} \approx 10^{13}$–10^{14}. The relative size of vacuum-state fluctuations in a multiparticle ensemble scales as $N^{-1/2}$. Therefore, all technical fluctuations of spins and light must be reduced to $\ll 10^{-6}$ before the vacuum-state noise level that is the benchmark for continuous-variable quantum-information processing can be reached. We achieve this by encoding quantum states of atoms and light at the high Larmor frequency $\Omega = 322$ kHz (the bias magnetic field of $B \approx 0.9$ G) where technical noise is much lower than at lower frequencies. This allows us to achieve vacuum (projection) noise level for atoms and vacuum (shot) noise level for light. Using the strong driving field also as the local oscillator field for polarization homodyne detection of photonic variables $y_{c,s}$ allows us to use detectors with nearly unity quantum efficiency.

The calibration of the input atomic spin state, the joint measurement, and the detection of the state teleported onto the spin B are performed using polarization homodyning measurements of the Stokes operator $S_2 = (n_{+45} - n_{-45})/2$ given by the difference of photon numbers polarized in $\pm 45°$ directions (Fig. 1)[22,24]. The measured canonical variable for light is then defined as $S_2 \approx \sqrt{\Phi}/2 \cdot y$, where Φ is the driving field photon flux, which experimentally means that all measurements are normalized to the shot noise of light. The photocurrent is analysed with a lock-in amplifier at Ω and further computer processed to obtain measurements of the temporal modes of interest $y_{c/s,-}$. Light pulses for teleportation and read-out always pass through both vapour cells (Fig. 1). For the read-out of each individual ensemble the other ensemble is detuned from the atom–light interaction by briefly detuning the B field in the respective cell. For off-resonant light well below saturation used here, the linear transformation of light variables after dispersive interaction with atoms is given by[20,24]:

$$y_{c/s,-} = \kappa \cdot p/x + c_y \cdot y^{in}_{c/s,f_y} + c_q \cdot q^{in}_{s/c,f_q} + c_N \cdot F_{p,x} \quad (1)$$

Here, the first term is a contribution of the atomic spin variable due to Faraday rotation of light polarization, the second term is proportional to the input value of the light quadrature y of the temporal mode f_y and the third term is the contribution of the other quadrature of input light q of temporal mode f_q resulting from back action of light on atoms (see Supplementary Information). All input light modes are always in a coherent or vacuum state with $\mathrm{Var}(y^{in}_{c/s,f_y}) = \mathrm{Var}(q^{in}_{c/s,f_q}) = 1/2$. The last term in equation (1) describes additional noise arising from atomic decoherence with $\mathrm{Var}(F_{p,x}) = m/2$, with $m = 1.3$ found from the atomic spin relaxation[25]. The value of the interaction constant κ is found by calibrating the Faraday rotation caused by the ensemble[20]. The constants c_y and c_q are determined by sending light with displacements of $\langle y^{in}_{c/s,f_y}\rangle$ and $\langle q^{in}_{c/s,f_q}\rangle$, storing it in the atomic medium, then reading it out onto another pulse $\langle y^{out}_{c/s,-}\rangle$ and measuring the ratios. The values for c_y, c_q and c_N can also be calculated (see Supplementary Information) using three experimental parameters: the total transverse decay rate of the atomic spin state γ, the contribution of spin decoherence (spontaneous emission, collisions and inhomogeneity of the magnetic field) to this decay rate γ_{extra} and $Z^2 = (\mu + \nu)/(\mu - \nu)$. $Z^2 = 6.3$ is calculated from Clebsch–Gordon coefficients for the atomic transitions and experimentally verified[21]. For 5.6 mW read-out pulses of 2 ms duration and room-temperature Cs vapour pressure (effective resonant optical depth of 34 for 22-mm-long cells) $\gamma = 99.3 \pm 0.2\ \mathrm{s}^{-1}$ and $\gamma_{extra} = 26.3 \pm 0.2\ \mathrm{s}^{-1}$ have been measured. A unitary contribution to the decay $\gamma - \gamma_{extra}$ is due to the collective coupling H_{int}, which describes the rate of entanglement generation and the beam-splitter interaction (see Supplementary Information) and depends on the optical depth of the ensemble, the optical detuning, and the intensity of the driving field. The measured values of κ, c_y, c_q agree very well with the predictions of the model (see Supplementary Information) and are $\kappa = 0.87$, $c_y = 0.93$, $c_q = 0.50$ for our teleportation setting. The last coefficient in the read-out equation can be found from the measured parameters as $c_N = c_q \cdot \sqrt{2 \cdot \gamma_{extra}/(\gamma - \gamma_{extra})}/Z = 0.17$. For the atomic-state reconstruction the detection efficiencies including optical losses $\eta_B = 0.80 \pm 0.03$ and $\eta_A = 0.89 \pm 0.03$ for ensembles A/B are taken into account.

Using equation (1) the mean values of the input states of ensemble A are found from measurements of light variables as $\langle x_A\rangle = \langle y^A_{c,-}\rangle/\kappa$, $\langle p_A\rangle = \langle y^A_{s,-}\rangle/\kappa$ and their variances as $\mathrm{Var}(x_A) = (\mathrm{Var}(y^A_{c,-}) - c_y^2/2 - c_q^2/2 - c_N^2 m/2)/\kappa^2$, $\mathrm{Var}(p_A) = (\mathrm{Var}(y^A_{s,-}) - c_y^2/2 - c_q^2/2 - c_N^2 m/2)/\kappa^2$. The prepared atomic input states are found to be very close to an ideal CSS with $\mathrm{Var}(x_A) = \mathrm{Var}(p_A) = (1.03 \pm 0.03) \cdot 1/2$, which confirms the validity of the read-out procedure. After each teleportation sequence, the mean values and the variances $\langle x^{tele}_B\rangle, \langle p^{tele}_B\rangle, \mathrm{Var}(x^{tele}_B), \mathrm{Var}(p^{tele}_B)$ of the spin state of the target ensemble B are found in the same way from the read-out of the verification pulse $y^B_{c/s,-}$. For CSS input states with displacements of $0, 5, 25, 160$ in canonical units and phases $0, \pi/4, \pi/2$ in x, p space, the variance of the teleported state showed no dependence on the displacement. The experimental fidelity is determined using a standard method of calculation of the state overlap (see Supplementary Information). Optimization of the teleportation protocol has been performed by varying the drive pulse duration T, the measured temporal mode of light, and the gain for the classical feedback. The optimal read-out mode was always found with an exponential decay rate equal to the spin decay γ as expected from the model.

Received 30 December 2012; accepted 15 April 2013; published online 2 June 2013

References

1. Briegel, H-J., Dür, W., Cirac, J. I. & Zoller, P. Quantum repeaters: The role of imperfect local operations in quantum communication. *Phys. Rev. Lett.* **81,** 5932–5935 (1998).
2. De Riedmatten, H. *et al.* Long distance quantum teleportation in a quantum relay configuration. *Phys. Rev. Lett.* **92,** 47904 (2004).
3. Gottesman, D. & Chuang, I. L. Demonstrating the viability of universal quantum computation using teleportation and single-qubit operations. *Nature* **402,** 390–393 (1999).
4. Gottesman, D., Kitaev, A. & Preskill, J. Encoding a qubit in an oscillator. *Phys. Rev. A* **64,** 012310 (2001).
5. Bennett, C. H. *et al.* Teleporting an unknown quantum state via dual classical and Einstein–Podolsky–Rosen channels. *Phys. Rev. Lett.* **70,** 1895–1899 (1993).
6. Vaidman, L. Teleportation of quantum states. *Phys. Rev. A* **49,** 1473–1476 (1994).
7. Bouwmeester, D. *et al.* A experimental quantum teleportation. *Nature* **390,** 575–579 (1997).
8. Furusawa, A. *et al.* Unconditional quantum teleportation. *Science* **282,** 706–709 (1998).
9. Riebe, M. *et al.* Deterministic quantum teleportation of atomic qubits. *Nature* **429,** 734–737 (2004).
10. Barrett, M. D. *et al.* Deterministic quantum teleportation with atoms. *Nature* **429,** 737–739 (2004).
11. Sherson, J. *et al.* Quantum teleportation between light and matter. *Nature* **443,** 557–560 (2006).
12. Chen, Y. A. *et al.* Memory-built-in quantum teleportation with photonic and atomic qubits. *Nature Phys.* **4,** 103–107 (2008).
13. Olmschenk, S. *et al.* Quantum teleportation between distant matter qubits. *Science* **323,** 486–489 (2009).
14. Nölleke, C. *et al.* Efficient teleportation between remote single-atom quantum memories. *Phys. Rev. Lett.* **110,** 140403 (2013).
15. Bao, X-H. *et al.* Quantum teleportation between remote atomic-ensemble quantum memories. *Proc. Natl Acad. Sci. USA* **109,** 20347–20351 (2012).
16. Duan, L. M., Lukin, M. D., Cirac, J. I. & Zoller, P. Long-distance quantum communication with atomic ensembles and linear optics. *Nature* **414,** 413–418 (2001).
17. Ma, X. S. *et al.* Quantum teleportation over 143 kilometres using active feed-forward. *Nature* **489,** 269–273 (2012).
18. Lee, N. *et al.* Teleportation of nonclassical wave packets of light. *Science* **332,** 330–333 (2011).
19. Hammerer, K., Sørensen, A. S. & Polzik, E. S. Quantum interface between light and atomic ensembles. *Rev. Mod. Phys.* **82,** 1041–1093 (2010).
20. Krauter, H. *et al.* Entanglement generated by dissipation and steady state entanglement of two macroscopic objects. *Phys. Rev. Lett.* **107,** 080503 (2011).

21. Wasilewski, W. *et al*. Generation of two-mode squeezed and entangled light in a single temporal and spatial mode. *Opt. Exp.* **17,** 14444–14457 (2009).
22. Sherson, J., Julsgaard, B. & Polzik, E. S. Deterministic atom-light quantum interface. *Adv. Atom. Mol. Opt. Phys.* **54,** 81–130 (2006).
23. Hammerer, K., Wolf, M. M., Polzik, E. S. & Cirac, J. I. Quantum benchmark for storage and transmission of coherent states. *Phys. Rev. Lett.* **94,** 150503 (2005).
24. Muschik, C. A. *et al*. Robust entanglement generation by reservoir engineering. *J. Phys. B* **45,** 124021 (2012).
25. Vasilyev, D. V., Hammerer, K., Korolev, N. & Sørensen, A. S. Quantum noise for Faraday light matter interfaces. *J. Phys. B* **45,** 124007 (2012).

Acknowledgements

We gratefully acknowledge discussions with J. I. Cirac, K. Hammerer and D. V. Vasilyev. This work was supported by the ERC grants INTERFACE and QUAGATUA, the Danish National Science Foundation Center QUANTOP, the DARPA programme QUASAR, the Alexander von Humboldt Foundation, TOQATA (FIS2008-00784) and the EU projects QESSENCE, MALICIA and AQUTE.

Author contributions

H.K., D.S., J.M.P., H.S. and T.F. performed the experiment. The theoretical model was developed by C.A.M. H.K, C.A.M., D.S. and E.S.P. wrote the paper. E.S.P. supervised the project.

Additional information

Supplementary information is available in the online version of the paper. Reprints and permissions information is available online at www.nature.com/reprints. Correspondence and requests for materials should be addressed to E.S.P.

Competing financial interests

The authors declare no competing financial interests.